Chemical Science

ROYAL SOCIETY OF CHEMISTRY

EDGE ARTICLE

View Article Online
View Journal | View Issue

Cite this: *Chem. Sci.*, 2024, **15**, 14037

All publication charges for this article have been paid for by the Royal Society of Chemistry

Received 10th June 2024
Accepted 1st August 2024

DOI: 10.1039/d4sc03797a

rsc.li/chemical-science

Supramolecular polymerization and bulk properties relationship in ester-functionalized *N*-annulated perylenediimides†

Lucía López-Gandul, [ab] Giulia Lavarda, [b] Bart W. L. van den Bersselaar, [b] Ghislaine Vantomme, [b] E. W. Meijer *[b] and Luis Sánchez *[a]

The synthesis of a series of *N*-annulated perylenediimides (NPDIs) **1–4** with an ester group and an alkyl spacer of different length in the peripheral chains was carried out, and the influence of the side chain architecture on the self-assembly, both in solution and in the solid state, was investigated. Solution studies evidenced that the carbonyl group plays a key role in the supramolecular organization of these derivatives, changing from an H-type isodesmic polymerization (**4**) to a J-type cooperative process as the spacer length decreases (**1–3**). On the other hand, bulk assays revealed an odd-even effect that correlates with the length of the alkyl spacer. Whereas the odd-spaced derivatives (**2** and **4**) organize in a disordered columnar hexagonal fashion, the even-spaced ones (**1** and **3**) show the formation of multiple crystalline (and liquid crystalline) structures. The results presented herein highlight the importance of side chain functionalization in the design of building blocks for in-solution and bulk purposes.

Introduction

In nature, self-assembly allows the achievement of complex and functional supramolecular structures in which the non-covalent interactions between relatively simple building blocks are crucial.[1] Prototypical examples of these natural self-assembled systems that inspire supramolecular chemists are collagen and the tertiary and quaternary structure of proteins.[2] To mimic this level of organization, the field of supramolecular polymers (*i.e.*, polymers composed of non-covalently linked monomeric units)[3–5] is experiencing a major development, finding applicability as biomaterials,[6] adhesives,[7] materials with enhanced mechanical properties,[8] or optoelectronic materials with improved efficiency.[9] The supramolecular polymerization of suitable monomeric species has been extensively investigated in solution.[3] However, self-assembly in solution may differ from that observed in the bulk material. In general, a high degree of organization can be achieved in solution by virtue of directional interactions such as H-bonding.[10] Contrarily, in bulk, the system has to strive to reduce the free volume. In this situation, weak non-covalent forces, such as van der Waals interactions between aliphatic chains play a relevant role in the formation of organized materials.[11]

In addition to external factors such as the nature of the solvent,[12] the supramolecular organization of monomeric species is strongly affected by the chemical structure of the molecular units. The impact of structural changes on the properties of self-assembled systems is generally dependent on the family of molecules under study, where small modifications in the molecular structure can translate into large changes in the self-assembly properties.[13] Particularly, the influence of monomer architecture on the supramolecular behaviour of *N*-annulated perylenediimides (NPDIs) has been studied by some of us.[14,15] The variation of the length of the linker tethering a central NPDI core to peripheral side chains endowed with amide functional groups has been shown to exert a remarkable influence on both the supramolecular polymerization mechanism and the morphology of the final aggregated species. However, a comparative study of the influence of the alkyl bridge length on the bulk properties is lacking. In addition to its relevance for comparative purposes, the investigation of supramolecular organization in bulk is relevant because the solvent-free synthesis of supramolecular polymers provides a more sustainable method to achieve highly organized, functional supramolecular structures, as recently reported by Aida and coworkers.[16]

Here, we present the synthesis and assembly of a series of NPDI derivatives (**1–4**, Fig. 1a) in which the peripheral trialkoxyphenyl moieties are linked to the aromatic core by an ester group. Despite the absence of inter- or intramolecular H-

[a]*Departamento de Química Orgánica, Facultad de Ciencias Químicas, Universidad Complutense de Madrid, 28040, Madrid, Spain. E-mail: lusamar@ucm.es*

[b]*Institute for Complex Molecular Systems, Laboratory of Macromolecular and Organic Chemistry, Eindhoven University of Technology, 5600 MB Eindhoven, The Netherlands. E-mail: E.W.Meijer@tue.nl*

† Electronic supplementary information (ESI) available. See DOI: https://doi.org/10.1039/d4sc03797a

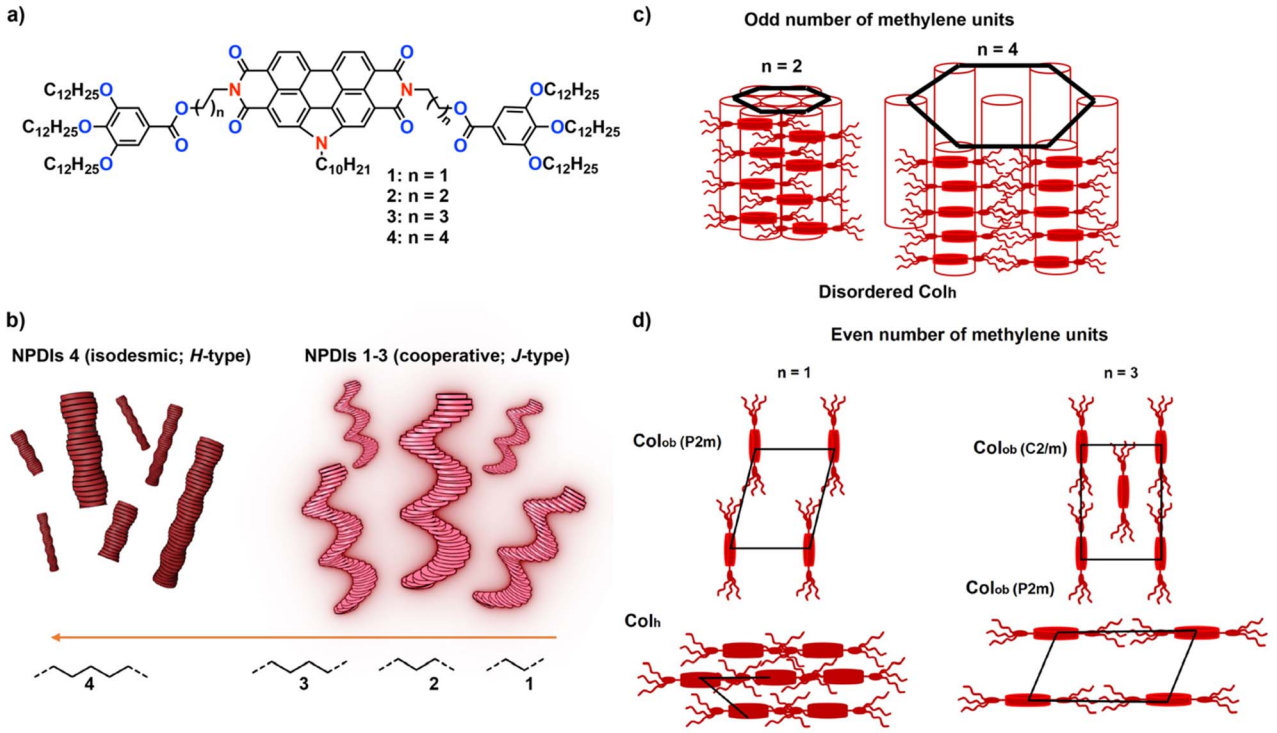

Fig. 1 (a) Chemical structures of NPDIs **1–4**. (b) Schematic representation of the in-solution assembly properties of compounds **1–4** as a function of the length of the spacer. (c/d) Schematic representation of the odd-even effect on the bulk packing of **1–4**.

bonding interactions, we demonstrate the ability of the investigated NPDIs to efficiently form supramolecular polymers in non-polar alkane solvents.[13a,17,18] The length of the alkyl bridge ester-functionalized NPDIs is found to exert a sharp influence on the self-assembly features of the investigated systems both in solution and in bulk (Fig. 1b–d), extending the knowledge of the structural rules that bias the supramolecular polymerization of electroactive units.

Results and discussion

Synthesis and self-assembly studies in solution

The synthesis of NPDIs **2–4** was carried out following a procedure similar to that reported for **1**.[17] This strategy consists of a convergent multistep synthesis involving a microwave-promoted reaction between the *N*-annulated perylene dianhydride **14** and the corresponding amino-ester precursor (**9.2–9.4**) in the presence of zinc acetate as catalyst and imidazole as base and solvent (Scheme S1†). All target NPDI derivatives were fully characterized by NMR, FT-IR spectroscopy and MALDI-HRMS (Experimental details are provided in the ESI†).

To investigate the ability of NPDIs **2–4** to form supramolecular polymers in solution, variable concentration (VC) ^{1}H NMR studies were first carried out (Fig. 2, S1 and S2†). In these experiments, an upfield shift of the resonances corresponding to the aromatic protons is observed with increasing concentration, suggesting π-stacking interaction between PDI cores. Further evidence for the stacking of the aromatic surfaces comes from the sharp changes in the coupling constants of the spin system attributable to the *ortho* and bay protons (namely, from AA′XX′ to AA′BB′, red and blue circles in Fig. 2) with increasing concentration. On the other hand, the small shifts in the resonances of the methylene units in the tether and those attached to the central nitrogen atom of the aromatic core are diagnostic of van der Waals interactions between these aliphatic units upon assembly (Fig. 2, S1 and S2†).

After assessing the nature of the non-covalent interactions driving the assembly of the investigated NPDIs in solution, variable temperature (VT) UV-Vis absorption studies were performed to elucidate the supramolecular polymerization mechanism of **2–4**. In agreement with the previously reported diester

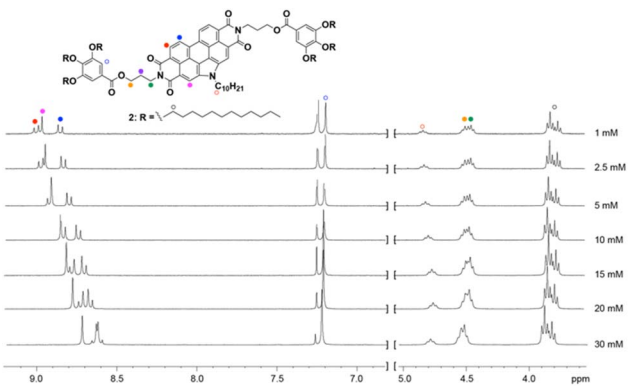

Fig. 2 Partial ^{1}H NMR spectra of NPDI **2** at different concentrations showing the changes in the aromatic and aliphatic resonances ($CDCl_3$, 300 MHz, 298 K).

1, the absorption spectra of compounds **2–4** in $CHCl_3$ show the typical absorption pattern of monomeric PDIs, with maxima at λ = 486 and 521 nm, attributed to the A_{0-1}/A_{0-0} transitions (Fig. 3a, c and S3†).[19] Similar spectra were obtained upon heating diluted solutions of the target NPDIs in MCH, being thus ascribed to molecularly dissolved species. Decreasing the temperature induces noticeable changes in the absorption pattern, which differ depending on the length of the linker connecting the trialkoxybenzoate units to the central aromatic core. A clear red shift of the absorption features is observed for NPDIs **2** and **3**, which show maxima at $\lambda = 602$ nm, diagnostic of the formation of aggregated J-type species (Fig. 3a, S3a and b†).[17] On the other hand, the emission spectra of assembled **2** and **3** in MCH show a clear increase in intensity compared to that of the monomeric species in $CHCl_3$, confirming the J-type nature of the supramolecular polymers formed (Fig. S4a and b†).[20]

To investigate whether the supramolecular polymerization of the target NPDIs in the investigated conditions is under thermodynamic control, cooling and heating absorption curves were measured with dilute solutions of **1–4** in MCH. A large thermal hysteresis was observed for NPDI **2**, along with a marked difference between the elongation and denaturation temperatures (Fig. S5a†). These observations are diagnostic of a kinetically controlled process.[21] In contrast, the thermal hysteresis in NPDIs **3** and **4** is negligible. Therefore, we assume that the supramolecular polymerization of these NPDIs is thermodynamically controlled (Fig. S5b and c†). The non-sigmoidal shape of the cooling curves obtained with dilute solutions of **3** in MCH is indicative of a cooperative supramolecular polymerization mechanism. A degree of cooperativity $\sigma = 6.7 \times 10^{-5}$ was derived from the model,[22] in agreement with that previously reported for NPDI **1** (Fig. 3b and S6†).[14] Interestingly, the K_e value derived for **3** is two orders of magnitude lower than that derived for **1**, indicating a lower stability of the supramolecular polymers formed.

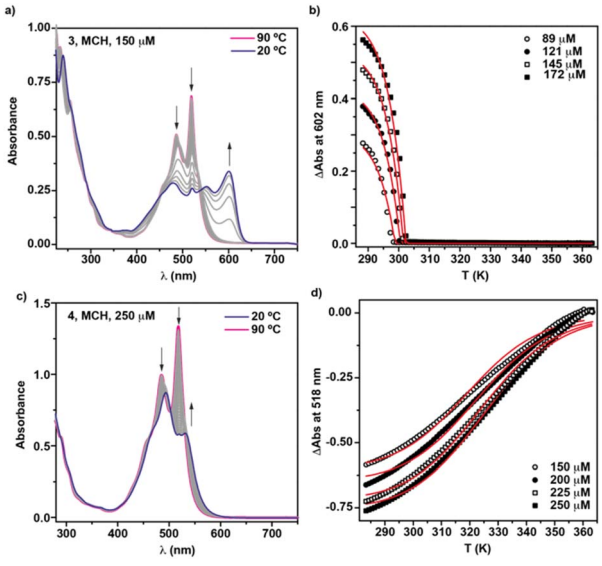

Fig. 3 (a and c) VT UV-Vis spectra of NPDIs **3** (a) and **4** (c) in MCH. (b and d) Plot of the variation of absorbance at specific wavelengths *versus* temperature for **3** (b) and **4** (d) at cooling rates of 1 K min^{-1}. The red traces in (c) and (d) depict the fitting of the equilibrium (EQ) model to the experimental curves.

On the other hand, the self-assembly of **4** in MCH presents remarkable differences from that observed for NPDIs **1–3**. In this case, a higher concentration is required to induce complete polymerization within the temperature range of study. In contrast to NPDIs **1–3**, the absorption pattern of the aggregated species of **4** shows a hypsochromic and hypochromic effect compared to the monomeric species, with a maximum at λ = 493 nm (Fig. 3c and S3c†). These absorption changes are characteristic of the formation of H-type aggregates, in which the aromatic units are arranged in a co-facial manner.[20] The sigmoidal shape of the cooling curves obtained at concentrations ranging from 150 to 250 μM suggests an isodesmic polymerization mechanism (Fig. 3d). Fitting the experimental cooling curves to the one-componet equilibrium model allowed the calculation of the thermodynamic parameters associated with the supramolecular polymerization of **4** (Table 1). The derived binding constant (namely, $K_a = 3.2 \times 10^4$ M^{-1}), confirms the lower stability of the aggregated species formed by **4** compared to NPDIs **1** and **2**. The similar emission intensity registered for solutions of **4** in MCH (aggregated species) and $CHCl_3$ (monomeric species) confirms the formation of H-type aggregates (Fig. S4c†).[20]

At this point, the morphology of the supramolecular polymers formed by assembly of NPDIs **2–4** was investigated by atomic force microscopy (AFM). Samples for AFM assays were prepared by spin-coating equilibrated solutions of the corresponding NPDI in MCH onto highly oriented pyrolytic graphite (HOPG) at 3000 rpm. The AFM images of **2** show a dense network of intertwined fibres (Fig. 4a, b and S7†). The formation of elongated structures is also observed in the AFM images of **3**. In this case, isolated thick fibres with typical heights of about 10 nm are observed along with large globular particles and a dense network of thinner and homogeneous fibres with heights of about 3.5 nm (Fig. 4c, d and S8†). Finally, the isodesmic supramolecular polymerization of **4** leads to the formation of nanoparticles with high polydispersity in height and diameter (Fig. 4e, f and S9†).

Overall, these results show that the ability of the monomer to self-assemble in solution increases as the distance between the carbonyl group of the peripheral chains and the central

Table 1 Thermodynamic parameters derived for the supramolecular polymerization of NPDIs **1**, **3** and **4** in MCH

	NPDI **1**[a]	NPDI **3**	NPDI **4**
ΔH_e (kJ mol^{-1})	-98.9 ± 1	-133.0 ± 1	-73.9 ± 1
ΔS (J K^{-1} mol^{-1})	-214 ± 2	-370 ± 2	-160 ± 3
ΔH_n (kJ mol^{-1})	-22.8 ± 1	-23.4 ± 1	—
σ (293 K)	8.3×10^{-5}	6.7×10^{-5}	1
K_e (M^{-1})	2.8×10^6	3.5×10^4	3.2×10^4
K_n (M^{-1})	2.4×10^2	2.31	—

[a] From ref. 13a.

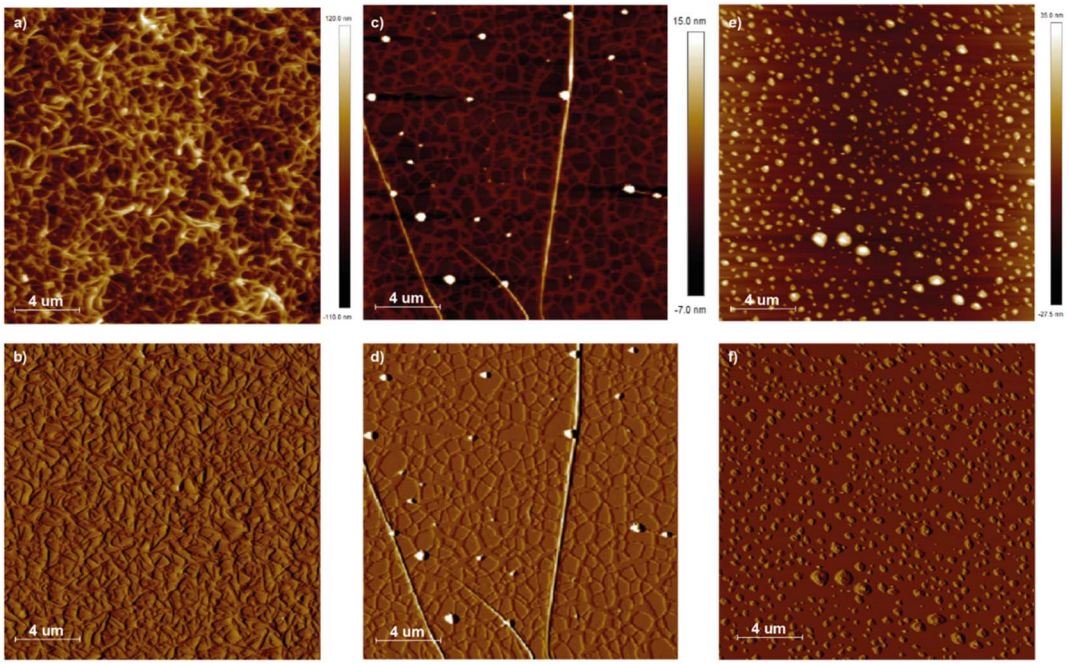

Fig. 4 Height (a, c and e) and phase (b, d and f) AFM images of NPDIs **2** (a, b, MCH, 100 μM); **3** (c, d, MCH, 150 μM) and **4** (e, f, MCH, 250 μM) onto HOPG as surface.

aromatic core decreases. Furthermore, the length of the linker also influences the supramolecular polymerization mechanism and the morphology of the polymeric species. These findings may be rationalized by taking into account the effect of the dipolar moment associated with the ester carbonyl group on the supramolecular polymerization process and its dependence on the length of the tether. It has been shown how the dipolar moment of the ester groups could act as an additional supramolecular interaction[13a] to the stacking and charge transfer interactions between NPDIs cores. This additional interaction increases the cooperativity of the self-assembly process as well as the strength of the assembly. We speculate that the flexibility of the longer bridge in **4** results in a less organized and less efficient self-assembly capability due to a lower contribution of the ester dipolar moment to the assembly. These findings are in good agreement with previous results observed for related chromophores in which the self-assembly is conditioned by the length of the linker connecting the central aromatic core and the peripheral side chains.[23]

Bulk studies

At this point, the bulk properties of **1–4** were investigated (Tables S1 and S2†). Differential scanning calorimetry (DSC) polarized optical microscopy (POM) and medium/wide-angle X-ray scattering (MAXS/WAXS) measurements were recorded to disclose the phase transitions of these materials and the nanomorphologies at different temperatures. DSC analysis of **1** showed two transitions upon cooling from 200 °C (Fig. 5a). The first one, at 175 °C, is identified as a disorder-order transition (T_{DOT}) based on the appearance of birefringent structures in the POM image and a distinct diffraction pattern in the MAXS/WAXS spectrum (Fig. 5b and S10†). Further cooling induced another thermal transition, which is assigned to an order–order phase transition (T_{OOT}) based on the low enthalpic contribution.[24] MAXS/WAXS experiments were used to elucidate the morphology of the phases corresponding to the different transition temperatures (Fig. 5b). In the scattering profile at 225 °C (yellow trace, Fig. 5b) only a single broad peak around 2.14 nm^{-1} is present, indicating that the material is in the isotropic state with a disordered feature of 2.93 nm. Upon cooling to 120 °C, multiple peaks are observed in the scattering pattern, corresponding to a columnar oblique (Col_{obl}) phase with *P*2*m* symmetry (Fig. 1c, see Table S2† for detailed calculations). The lattice parameters were determined to be $a = 3.4$ nm and $b = 3.9$ nm with an oblique angle of $\gamma = 86°$. Further cooling to 25 °C induces an order–order transition from the previously observed Col_{obl} to a columnar hexagonal (Col_h) phase with $a = 3.2$ nm (Fig. S10, Tables S1 and S2†).

In the case of NPDI **2**, which comprises three methylene units in the linker, only one sharp transition is visible in the DSC trace (Fig. 5c). This corresponds to the isotropic melt–solid transition, as indicated by MAXS/WAXS experiments (Fig. 5d). Herein, the formation of a Col_h phase with a domain spacing of 3.3 nm is evident at room temperature, while an isotropic state is reached at 200 °C. As visible in the POM images (Fig. S11†), almost no birefringence is observed at 200 °C, confirming that the resulting solid structure does not exhibit a high degree of order and in line with the broad peaks observed in the MAXS/WAXS traces (Fig. S11 and Table S1†).

Similar to NPDI **1**, which also contains an even-numbered methylene bridge, the DSC trace of **3** shows multiple phase transitions upon cooling from 200 °C (Fig. 5e). The first one is

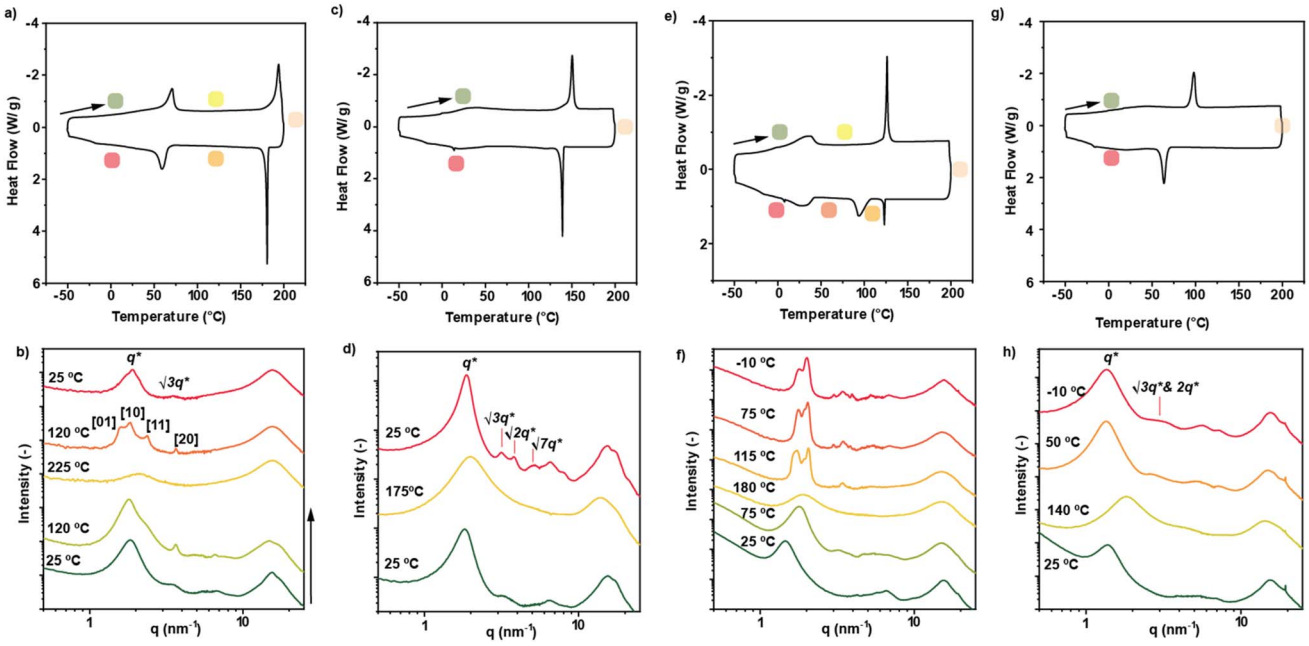

Fig. 5 (a, c, e and g) DSC traces of NPDIs **1** (a), **2** (c), **3** (e) and **4** (g) obtained with a rate of 5 K min^{-1}. Colored squares correspond to the different phases observed. (b, d, f and h) 1D transmission scattering profiles at different temperatures of **1** (b), **2** (d), **3** (f) and **4** (h).

related to a disorder–order transition to a liquid crystalline phase based on the observed scattering pattern in MAXS/WAXS and the shearability of the sample in POM (Fig. 5f and S12a†). The unit parameters of this Col_{obl} phase were calculated as a = 3.5 nm, b = 3.9 nm and $\gamma = 69°$. These values are very similar to those observed for **1**, indicating a comparable bulk packing between **1** and **3**. The small difference in a can be rationalized considering the two additional methylene units in **3**. Further cooling to 75 °C results in a slightly tighter packing of the same Col_{obl} phase (Tables S1 and S2†), which is supported by the similarities in the MAXS/WAXS spectra and POM images (Fig. 5f and S12c†). Finally, cooling to −10 °C reveals an order–order transition to a $C2/m$ symmetric Col_{obl} phase with unit parameters of a = 3.5 nm, b = 7.1 nm and $\gamma = 82°$ (Fig. 1c, S13 and S14†). A clear change in the birefringent textures is visible at −10 °C, corroborating the aforementioned order–order transition (Fig. S12†). The data obtained from the bulk studies for **1** and **3** correlates with the results obtained in solution, since the packing of both these structures in MCH forms *J*-aggregates. Furthermore, it is worthy to mention that the AFM images of NPDI **3** display the formation of aggregates of multiple morphologies. In fact, the formation of both disk-like micelles and long fibers (Fig. 4c and d) could be directly related to the above-mentioned multiple packing mechanisms observed in bulk (Fig. 5e and f).

Finally, the bulk properties of **4** were investigated. In this case, the results are comparable to those obtained for compound **2**. Controlled cooling from the isotropic state (Fig. 5g and h, yellow trace) results in a Col_h packing (Fig. 5g and h, red trace) with a lattice parameter of a = 4.6 nm. It is worth noting that the domain spacing increases significantly from derivative **2** to **4** (namely, from 3.3 nm to 4.6 nm). Such increase is larger than solely the additional length of four carbon atoms. This suggest that the packing of these two derivatives is slightly different at room temperature, which is confirmed by the fact that only **4** displays a weak scattering peak at 19.4 nm^{-1}. This reflection corresponds to a distance of 3.2 Å, which is typically observed in π-stacked systems. Since the presence of aromatic interactions has previously been assigned to unimolecular stacks, we assume a similar assembly for these *N*-annulated PDIs.[25] We hypothesize that NPDI **2** shows more intercalation of the wedges compared to **4**, leading to a decrease in domain spacing and less efficient NPDI–NPDI interactions, explaining the absence of this reflection associated with π-stacking (Fig. 1c). This fact is also consistent with the observed aggregation in solution, as **2** assembles into J-type aggregates, where π-stacking is less efficient due to the stair-like nature of the assembly. In contrast, **4** self-assembles into H-type aggregates, in which the monomers are arranged in a cofacial fashion, resulting in more efficient aromatic stacking.

Overall, the bulk characterization of NPDIs **1**–**4** shows an odd-even effect, where only NPDIs with an even number of methylene units in their bridge (**1** and **3**, respectively) exhibit multiple phase transitions with well-defined structures. We hypothesize that the origin of the odd-even effect is related to the asymmetry of the core, with different lengths of the spacer causing the wedges to be present at different proximities to the bay functionalization, thus affecting the stacking and crystallization of the PDI.

Conclusions

In this work, we present a systematic investigation of the influence of alkyl side chain length on the assembly behaviour

of NPDIs functionalized with ester groups in solution and in bulk. Spectroscopic studies in solution showed that the system behaves more cooperatively and assembles with a higher equilibrium constant as the spacer length decreases. We relate this effect to the dipole–dipole interaction provided by the carbonyl group, which adds up to the stacking of the aromatic PDI cores in driving the assembly. Thus, while **4** assembles *via* an isodesmic mechanism to yield H-type aggregates, NPDIs **1–3** self-assemble in a cooperative manner to afford highly emissive J-type assemblies. On the other hand, bulk studies showed an odd-even effect in the assembly properties of the investigated derivatives. NPDIs **1** and **3** (endowed with an even number of methylene units) exhibit liquid crystalline phase behaviour with multiple thermal transitions, while forming columnar oblique packings. In contrast, NPDIs **2** and **4** (featuring a linker with an odd number of methylene groups) exhibit single thermal transitions, below which they arrange into columnar hexagonal phases. The increase in domain spacing between **2** and **4** is larger than the difference in length between the respective side chains, indicating a more efficient aromatic interaction in the latter and a higher wedge intercalation in the former.

This study sheds light on the importance of molecular design in determining the architectures of NPDI-based supramolecular assemblies.

Data availability

The data that supports the findings of this study have been included in the main text and ESI† and are available from the corresponding authors upon reasonable request.

Author contributions

Lucía López-Gandul: synthesis of the NPDIs, in-solution studies, AFM imaging, DSC measurements, POM imaging and writing; Giulia Lavarda: supervision and writing; Bart van den Bersselaar: SAXS measurements and writing; Ghislaine Vantomme, E. W. Meijer and Luis Sánchez: conceptualization, writing, supervision, and funding acquisition.

Conflicts of interest

There are no conflicts to declare.

Acknowledgements

Financial support by the MCIN/AEI of Spain (PID2020-113512GB-I00 and TED2021-130285B-I00) is acknowledged. G. L. acknowledges a Marie Skłodowska-Curie Postdoctoral Individual Fellowship (101026072) for financial support. Also supported by the European Research Council (SYNMAT project ID 788618) and the Dutch Ministry of Education, Culture and Science (Gravity program 024.001.035).

Notes and references

1 (*a*) S. Mann, *Nature*, 1993, **365**, 499; (*b*) L.-J. Chen and H.-B. Yang, *Acc. Chem. Res.*, 2018, **51**, 2699.
2 (*a*) D. R. Eyre, *Science*, 1980, **207**, 1315; (*b*) A. Bhattacharjee and M. Bansal, *IUBMB Life*, 2005, **57**, 161; (*c*) J. Kyte in *Structure in Protein Chemistry*, Garland Publishing, New York, 1995.
3 (*a*) T. F. A. De Greef, M. M. J. Smulders, M. Wolffs, A. P. H. J. Schenning, R. P. Sijbesma and E. W. Meijer, *Chem. Rev.*, 2009, **109**, 5687; (*b*) M. Wehner and F. Würthner, *Nat. Rev. Chem*, 2020, **4**, 38.
4 T. Aida, E. W. Meijer and S. Stupp, *Science*, 2012, **335**(6070), 813–817.
5 T. Aida and E. W. Meijer, *Isr. J. Chem.*, 2020, **60**, 33–47.
6 (*a*) Z. Álvarez, A. N. Kolberg-Edelbrock, I. R. Sasselli, J. A. Ortega, R. Qiu, Z. Syrgiannis, P. A. Mirau, F. Chen, S. M. Chin, S. Weigand, E. Kiskinis and S. I. Stupp, *Science*, 2021, **374**, 848; (*b*) O. Dumele, L. ordević, H. Sai, T. J. Cotey, M. H. Sangji, K. Sato, A. J. Dannenhoffer and S. I. Stupp, *J. Am. Chem. Soc.*, 2022, **144**, 3127.
7 W. Zhao, J. Tropp, B. Qiao, M. Pink, J. D. Azoulay and A. H. Flood, *J. Am. Chem. Soc.*, 2020, **142**, 2579.
8 R. P. Sijbesma, F. H. Beijer, L. Brunsveld, B. J. B. Folmer, K. J. H. K. Hirschberg, R. F. M. Lange, J. K. L. Lowe and E. W. Meijer, *Science*, 1997, **278**, 1601.
9 (*a*) Y. Yanagisawa, Y. Nan, K. Okuro and T. Aida, *Science*, 2018, **359**, 72; (*b*) Y. Yamamoto, T. Fukushima, Y. Suna, N. Ishii, A. Saeki, S. Seki, S. Tagawa, M. Taniguchi, T. Kawai and T. Aida, *Science*, 2006, **314**, 1761; (*c*) R. Rodríguez, C. Naranjo, A. Kumar, P. Matozzo, T. Kumar Das, Q. Zhu, N. Vanthuyne, R. Gómez, R. Naaman, L. Sánchez and J. Crassous, *J. Am. Chem. Soc.*, 2022, **144**, 7709.
10 S. Cantekin, T. F. A de Greef and A. Palmans, *Chem. Soc. Rev.*, 2012, **41**, 3125–6137.
11 L. N. J. de Windt, Z. Fernández, M. Fernández-Míguez, F. Freire and A. R. A. Palmans, *Chem.–Eur. J.*, 2022, **28**, e202103691.
12 M. F. J. Mabesoone, A. R. A. Palmans and E. W. Meijer, *J. Am. Chem. Soc.*, 2020, **142**, 19781.
13 (*a*) M. A. Martínez, A. Doncel-Giménez, J. Cerdá, J. Calbo, R. Rodríguez, J. Aragó, J. Crassous, E. Ortí and L. Sánchez, *J. Am. Chem. Soc.*, 2021, **143**, 13281; (*b*) K. Tashiro, K. Katayama, K. Tamaki, L. Pesce, N. Shimizu, H. Takagi, R. Haruki, M. J. Hollamby, G. M. Pavan and S. Yagai, *Angew. Chem., Int. Ed.*, 2021, **60**, 26986.
14 S. Ogi, V. Stepanenko, J. Thein and F. Würthner, *J. Am. Chem. Soc.*, 2016, **138**, 670.
15 (*a*) E. E. Greciano, M. A. Martínez, S. Alsina, A. Laguna and L. Sánchez, *Org. Chem. Front.*, 2021, **8**, 5328; (*b*) C. Naranjo, S. Adalid, R. Gómez and L. Sánchez, *Angew. Chem., Int. Ed.*, 2023, **62**, e202218572.
16 Z. C. Y. Suzuki, A. Imayoshi, X. Ji, K. V. Rao, Y. Omata, D. Miyajima, E. Sato, A. Nihonyanagi and T. Aida, *Nat. Mater.*, 2022, **21**, 253.

17 E. E. Greciano, J. Calbo, E. Ortí and L. Sánchez, *Angew. Chem., Int. Ed.*, 2020, **59**, 17517.
18 (*a*) I. Hisaki, H. Shigemitsu, Y. Sakamoto, Y. Hasegawa, Y. Okajima, K. Nakano, N. Tohnai and M. Miyata, *Angew. Chem., Int. Ed.*, 2009, **48**, 5465; (*b*) H. Shigemitsu, I. Hisaki, E. Kometani, D. Yasumiya, Y. Sakamoto, K. Osaka, T. S. Thakur, A. Saeki, S. Seki, F. Kimura, T. Kimura, N. Tohnai and M. Miyata, *Chem.–Eur. J.*, 2013, **19**, 15366; (*c*) H. Shigemitsu, I. Hisaki, H. Senga, D. Yasumiya, T. S. Thakur, A. Saeki, S. Seki, N. Tohnai and M. Miyata, *Chem.–Asian J.*, 2013, **8**, 1372.
19 F. Würthner, C. R. Saha-Möller, B. Fimmel, S. Ogi, P. Leowanawat and D. Schmidt, *Chem. Soc. Rev.*, 2016, **116**, 962.
20 F. Würthner, T. E. Kaiser and C. R. Saha-Möller, *Angew. Chem., Int. Ed.*, 2011, **50**, 3376.
21 (*a*) S. Ogi, V. Stepanenko, K. Sugiyasu, M. Takeuchi and F. Würthner, *J. Am. Chem. Soc.*, 2015, **137**, 3300; (*b*) C. Naranjo, S. Adalid, R. Gómez and L. Sánchez, *Angew. Chem., Int. Ed.*, 2023, **62**, e202218572; (*c*) E. E. Greciano, S. Alsina, G. Ghosh, G. Fernández and L. Sánchez, *Small Methods*, 2020, **4**, 1900715.
22 H. M. M. ten Eikelder, A. J. Markvoort, T. F. A. de Greef and P. A. J. Hilbers, *J. Phys. Chem. B*, 2012, **116**, 5291.
23 (*a*) T. Seki, S. Yagai, T. Karatsu and A. Kitamura, *J. Org. Chem.*, 2008, **73**, 3328; (*b*) D. D. Günbas, C. Xue, S. Patwardhan, M. C. Fravventura, H. Zhang, W. F. Jager, E. J. R. Sudhölter, L. D. A. Siebbeles, T. J. Savenije, S. Jin and F. C. Grozema, *Chem. Commun.*, 2014, **50**, 4955.
24 S. Lee, T. M. Gillard and F. S. Bates, *AIChE J.*, 2013, **59**, 3502.
25 (*a*) F. Würthner, C. Thalacker, S. Diele and C. Tschierske, *Chem.–Eur. J.*, 2001, **10**, 2245; (*b*) V. Percec, M. Peterca, T. Tadjiev, X. Zeng, G. Ungar, P. Leowanawat, E. Aqad, M. R. Imam, B. M. Rosen, U. Akbey, R. Graf, S. Sekharan, D. Sebastiani, H. W. Spiess, P. A. Heiney and S. D. Hudson, *J. Am. Chem. Soc.*, 2011, **133**, 12197; (*c*) R. H. Zha, G. Vantomme, J. A. Berrocal, R. Gosens, B. de Waal, S. Meskers and E. W. Meijer, *Adv. Funct. Mater.*, 2018, **28**, 1703952.